ADVANCED FUNCTIONAL MATERIALS
www.afm-journal.de

Materials Views
www.MaterialsViews.com

Effects of Divalent Metals on Nanoscopic Fiber Formation and Small Molecule Recognition of Helical Proteins

*Susheel K. Gunasekar, Luona Anjia, Hiroshi Matsui, and Jin K. Montclare**

Metal dependent protein-based assemblies derived from the cartilage oligomeric matrix protein (C) coiled-coil domain (His_6-C) and two variants with mutation at position 40 (His_6-T40A) and 44 (His_6-L44A) are explored. All proteins have an N-terminal hexahistidine tag (His_6) that interacts with divalent metal ions Zn(II) and Ni(II). Binding to Zn(II) confers enhanced helical structure and stability, while Ni(II) promotes aggregation. Surprisingly, His_6-L44A undergoes a conformational switch from unstructured to α-helix in the presence of Zn(II). Both His_6-C and His_6-T40A further assemble into discrete nanofibers that appear to be stabilized by Zn(II) in which the fiber formation is dictated by the α-helical content. Because Ni(II) promotes aggregation, the proteins visibly cluster, forming large fiber mats in the case of His_6-C and His_6-T40A or aggregated structures as observed for His_6-L44A. Due to the unique pentameric assembly of the proteins, recognition of a small molecule within the pore is assessed using curcumin as the guest molecule. In the presence of Zn(II), there is enhanced binding to curcumin, while the addition of Ni(II) causes a loss in binding. It is shown that metal binding serves as a trigger to control the conformation of the proteins, affecting the nanoscopic fibrous assemblies and small molecule recognition abilities.

1. Introduction

Protein/peptide nanostructures capable of assembling into detailed macromolecular complexes by bottom-up approaches have potential applications in catalysis, light harvesting, optics, and electronics.[1–6] Motifs that can undergo a conformational switch due to external changes in pH, temperature, small molecules, and metals have been exploited to control self-assembly patterns.[7–11] This external trigger mechanism can serve as a tool for designing nanostructures with precise conformation and dimensions. In particular, metals can have a macroscopic effect on protein folding and stability upon binding.[10,12]

Divalent metals such as Cu(II), Zn(II), and Ni(II) have been shown to mediate conformational changes upon binding to His residues within proteins and polypeptides.[12–15] The Woolfson group designed a peptide, ZiCo, to switch between a coiled-coil to zinc finger type motif upon binding to Zn(II).[12] Ulrich and coworkers studied an 18-residue long peptide (B18) isolated from the sea urchin fertilization protein bindin, which is known to mediate vesicle aggregation and membrane fusion. This peptide transformed from random to α-helical structure when bound to Zn(II) and mimicked the function of the parent protein.[13] In another study, Tanaka and colleagues demonstrated that a de novo designed peptide (IZ-3aH) can differentially bind divalent metals, exhibiting affinity towards Cu(II) and Zn(II) and assembling into a triple stranded coiled-coil but incapable of binding Ni(II).[14] Most recently, Signarvic and DeGrado introduced metal binding sites at the *i* and *i* + 4 positions of the wasp venom lytic peptide mastoparan X. While addition of Zn(II) did not affect the structure or lytic ability of one of the designed peptides, Mst-HAH, Ni(II) binding promoted helix formation and hemolysis.[15]

While these studies on metal-dependent folding and binding have been focused on sequences in which His residues are placed within the polypeptide at specified distances, here we explore the impact of Zn(II) and Ni(II) on helical coiled-coil and random coil polypeptides bearing an N-terminal hexahistidine (His_6) sequence.[10,12–16] Specifically we investigate the effect of these divalent metals on three polypeptides derived from the cartilage oligomeric matrix protein (C) coiled-coil domain (His_6- C) and two variants with mutation at position 40 (His_6-T40A) and 44 (His_6-L44A) (**Scheme 1**).[16] The His_6-T40A in the absence of any metals

S. K. Gunasekar, Dr. J. K. Montclare
Department of Chemical and Biological Sciences
Polytechnic Institute of New York University
Brooklyn, NY 11201, USA
E-mail: jmontcla@poly.edu
L. Anjia, Dr. H. Matsui
Department of Chemistry and Biochemistry at Hunter College
The City University of New York
New York, NY 10065, USA
Dr. J. K. Montclare
Department of Biochemistry
SUNY Downstate Medical Center
Brooklyn, NY 11203, USA

DOI: 10.1002/adfm.201101627

a b c d e f g a b c d e f g a b c d e f g a b c d e f g a b c d e f g

His_6-C	MRGSHHHHHHGSDLAPQMLREIQETNAAIQDVRELIRQQVKE/TFIKNTVMESDASGKLN
His_6-T40A	MRGSHHHHHHGSDLAPQMLREIQEANAAIQDVRELIRQQVKE/TFIKNTVMESDASGKLN
His_6-L44A	MRGSHHHHHHGSDLAPQMLREIQETNAAAQDVRELIRQQVKE/TFIKNTVMESDASGKLN

Scheme 1. Protein sequence of His_6-C, His_6-T40A, and His_6-L44A with the residues at the *a* and *d* positions highlighted.

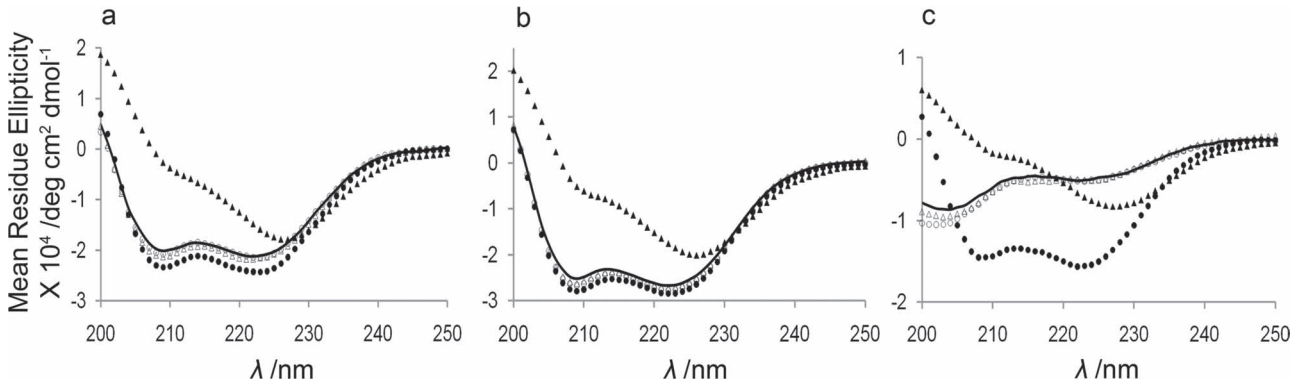

Figure 1. Wavelength scans of a) His_6-C, b) His_6-T40A, and c) His_6-L44A protein (solid black lines), in the presence of zinc (closed circles), in the presence of zinc and EDTA (open circles), in the presence of nickel (closed triangles), and in the presence of nickel and EDTA (open triangles).

exhibit a highly structured and stable coiled-coil relative to His_6-C, while His_6-L44A reveals a random coil structure incapable of forming pentameric assemblies.[16] Our studies demonstrate differential binding of Zn(II) and Ni(II) to our proteins and its influence on the nanoscopic fiber assembly and small molecule recognition.

2. Results and Discussion

2.1. Differential Effects of Zn(II) and Ni(II) on Conformation and Stability

Initially, to assess both secondary structure and thermal stability of all proteins in the absence and presence of Zn(II) and Ni(II), circular dichroism (CD) studies were performed (**Figure 1**, Supporting Information Table S1). The His_6-C possesses a distinctive double minima at 208 and 222 nm, indicative of an α-helix with a helical content of 55% (Figure 1a). Monitoring the mean molar residue ellipticity signal at Θ_{222} as a function of temperature, His_6-C reveals a fully reversible temperature-dependent curve with a thermal mid-point of transition (T_m) of 48 °C, which is consistent with previously determined values.[16] In the presence of 100 μM of Zn(II), there is an increase in the helical content to 63% along with a drastic increase in stability (T_m > 80 °C). By contrast, a large loss in the minimum at 208 nm and a red shift of the 222 nm minimum to 224–225 nm is observed in the presence of 100 μM of Ni(II) (Figure 1a, Supporting Information Table S1). This phenomenon is indicative of formation of higher order aggregates and particulate systems.[1,17,18] While an overall loss in helical content to 38% is observed for His_6-C, there is a 15 °C increase in T_m (Figure 1a, Supporting Information Table S1). Upon chelation of Zn(II) and Ni(II) with 1 mM of ethylenediaminetetraacetic acid (EDTA), the secondary structure returns to its original state with similar helical content and T_m of His_6-C in the absence of metals (Figure 1a, Supporting Information Table S1).

For His_6-T40A, the total helical content is 69% with a T_m of 62 °C, similar to the values reported earlier (Figure 1b, Supporting Information Table S1).[16] The presence of 100 μM of Zn(II) increases the T_m drastically (>80 °C) with an overall helical content of 74%. A loss in minimum at 208 nm alongside a red shift of the minimum at 222 nm to 224–225 nm is observed upon Ni(II) binding, similar to the His_6-C. A loss in helical content to 45% is observed in the presence of Ni(II). In spite of the overall reduction in α-helical content, a 6 °C increase in T_m was observed (Figure 1b, Supporting Information Table S1). The addition of 1 mM EDTA for His_6-T40A in the presence of Zn(II) and Ni(II) led to reversion to its original structural and thermal properties.

Finally, the wavelength spectra of His_6-L44A reveal a random coil conformation (Figure 1c). Unlike the previous two proteins, His_6-L44A has a very low helical content of just 13% and is thermally unstable (Figure 1c, Supporting Information Table S1). However, addition of Zn(II) changes the conformation of the protein from random coil to α-helix, as evident from the presence of a double minima at 208 and 222 nm (Figure 1c, Supporting Information Table S1). In addition, there is a steep increase in helical content (40%) as well as the observation of a discernible melting point (72 °C). The His_6-L44A exhibits a reversible structure and thermal denaturation curve, indicating that the Zn(II)- mediated folding stabilizes the helical structure. Ni(II) effects His_6-L44A in a different way than Zn(II) in which there is a loss in 208 nm minimum and red shift of the 222 nm minimum to 224–225 nm, indicative of aggregation (Figure 1c, Supporting Information Table S1). Although the overall helical content is 17%, there is a considerable increase in the thermal stability of the protein (58 °C) (Figure 1c, Supporting Information Table S1). In the presence of EDTA, His_6-L44A reverts to its original random coil structure and loss of thermal stability.

As a control, the His_6-tag was removed from all proteins through the incorporation of a factor Xa cleavage site (Supporting Information Scheme S1, Figure S3). The resulting proteins, without the His_6-tag, exhibit no significant change in structure in the presence of Zn(II) or Ni(II) suggesting that the presence of the tag is necessary for binding and subsequent effects on molecular organization/assembly. Thus, these studies indicate that Zn(II) and Ni(II) induce different conformation and stability profile for all proteins bearing the N-terminal hexahisitidine tag.

Table 1. Summary of ITC data.

Protein	Zn (II)			Ni (II)		
	N (number of sites)	K_d [μM]	ΔH [kcal mol^{-1}]	N (number of sites)	K_d [μM]	ΔH [kcal mol^{-1}]
His_6-C	2.1	2.1	–4.6	0.3	1.9	–12.6
His_6-T40A	2.9	7.6	–9.5	0.3	2.5	–47.9
His_6-L44A	4.0	1.3	–5.9	0.9	2.8	–9.8

2.2. Thermodynamic Analysis of Metal Binding

The quantitative binding of the proteins to Zn(II) and Ni(II) are assessed via isothermal titration calorimetry (ITC). All proteins bind both metals with dissociation constants (K_d) in the μM range (**Table 1**, Supporting Information Figure S4). His_6-C demonstrate essentially comparable binding to both metals with of K_d values of 2.1 ± 0.1 μM and 1.9 ± 0.2 μM for Zn(II) and Ni(II), respectively. By contrast, His_6-T40A illustrates a distinct preference for Ni(II) over Zn(II) with K_d values of 2.5 ± 0.1 μM and 7.6 ± 1.9 μM for Ni(II) and Zn(II), respectively. Finally, His_6-L44A reveals opposite binding preference to that of His_6-T40A; it binds better to Zn(II) with a K_d of 1.3 ± 0.4 μM relative to Ni(II) (K_d = 2.8 ± 0.9 μM). In addition to determining affinities, the molar ratios for Zn(II) and Ni(II) are evaluated. For Zn(II) binding, His_6-C, His_6-T40A, and His_6-L44A indicate molar ratios of 2, 3,and 4, respectively (Table 1). Thus, multiple Zn(II) ions can be coordinated by each protein monomer chain in an interstrand fashion, which can subsequently induce helical structure and assembly. In the case of Ni(II), the molar ratios are below 1 for all three proteins (Table 1); this suggests that several protein monomers coordinate to a single Ni(II) leading to intrastand interactions consistent with the observed macrosopic aggregation.

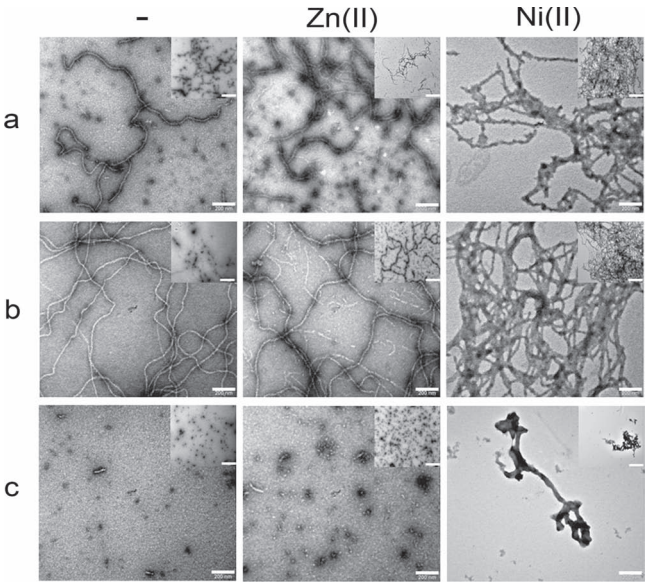

Figure 2. TEM images of a) His_6-C, b) His_6-T40A, and c) His_6-L44A in the absence (-) and presence of Zn(II) and Ni(II) metals. Scale bars represents 200 nm in the figure and 1 μm in the insets.

2.3. Conformation-Dependent Fiber Formation as a Function of Metals

Transmission electron microscopy (TEM) studies are performed to determine the supramolecular assemblies of the proteins in the absence and presence of metals. Remarkably, His_6-C self-assembles into fiber-like structures several micrometers in length with an average diameter between 10–15 nm, in the absence of metals (**Figure 2**a). The fiber dimension is further confirmed via small angle X-ray scattering (SAXS) in which the fit to cylindrical form factor yields a diameter size of 12 nm (**Figure 3**a).[19,20] In addition to linear fibers, there are particles with an average diameter of 20 nm. In the presence of Zn(II), the fibers interact with one another and are moderately aggregated; the fiber dimensions of the individual strands remain consistent to those in the absence of metal. In the presence of Ni(II), the fibers assemble into micrometer sized aggregates, confirming that Ni(II) induces aggregation. For His_6-T40A, the fibers are formed very similar to the His_6-C in which the fibers are 10–15 nm in diameter and microns in length (Figure 2b). The calculated SAXS diameter is 14 nm, consistent with TEM (Figure 3b).[19,20] In general, a greater number of fibers are observed for His_6-T40A than His_6-C, suggesting that the enhanced helicity and stability of His_6-T40A leads to the formation of more robust fibers. Furthermore, there are no visible particles of His_6-T40A that have been observed for His_6-C. Addition of Zn(II) leads to moderate aggregation while addition of Ni(II) causes higher order aggregates. His_6-L44A, which is incapable of forming α-helical structures, exhibits particles of ≈25 nm in diameter in the absence and presence of metals (Figure 2c). Although Zn(II) induces helical structure to His-L44A, it is not sufficient for the fiber formation as only particles are observed. In the presence of Ni(II), the particles are aggregated into micrometer-sized amorphous structures (Figure 2c).

2.4. Conformation of Fibers in the Solid State

To further validate that the fibers observed in TEM are indeed due to the α-helical conformation, we analyzed the protein structures in the solid state via attenuated total reflection Fourier transform infrared (ATR-FTIR) spectroscopy in the presence of phosphate buffer (PB) and partial deuterium oxide (D_2O) exchange (**Table 2**). Irrespective of PB or D_2O, both His_6-C and His_6-T40A exhibits an amide I peak between 1653 cm^{-1} in the

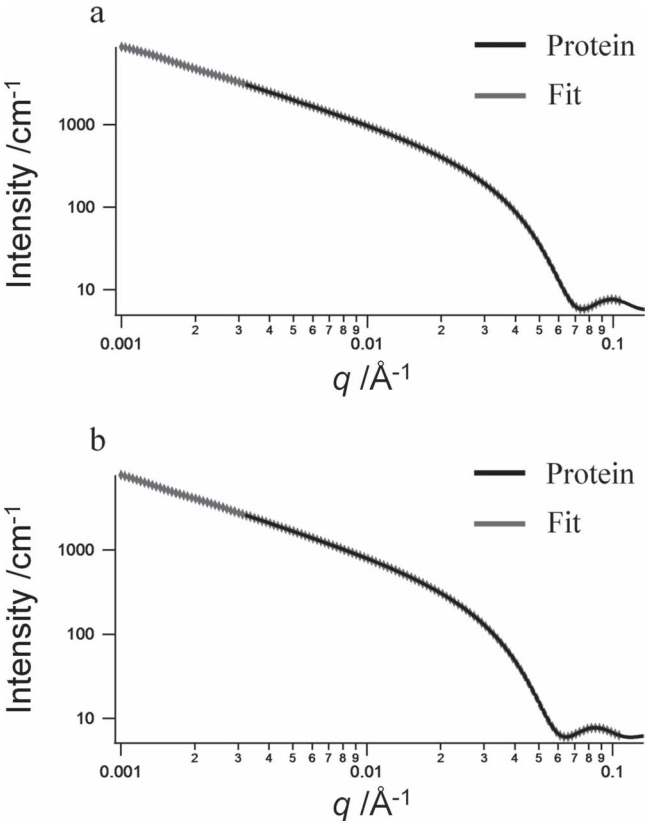

Figure 3. Curve-fitting of SAXS of a) His_6-C and b) His_6-T40A to cylinder model.

absence and presence of metals, demonstrating that the fibers are indeed α-helical (Supporting Information Figure S5).[21] The spectra of His_6-L44A possesses a peak at 1653 cm^{-1} in the presence of PB whereas in the presence of D_2O, it possesses two peaks at 1647 and 1652 cm^{-1}, indicating the presence of random coil content (Supporting Information Figure S5, Table 2).[21,22] Addition of Zn(II) and Ni(II) resulted in a single peak in PB at 1653 cm^{-1} for all proteins (Supporting Information Figure S6, S7). In D_2O exchange conditions, a major peak at 1653 cm^{-1} with a small shoulder at 1648 cm^{-1} were present in the presence of Zn(II), while for Ni(II), a major peak at 1653 cm^{-1} with a shoulder at 1647 cm^{-1} were present. Under both Zn(II) and Ni(II) conditions exclusively, the proteins aggregate into visible particles. Thus the shoulder peaks at 1648 and 1647 cm^{-1} arising in the presence of metals is likely due to the disordered aggregates (Supporting Information Figure S6, S7, Table 2).[23,24]

2.5. Metal-Dependent Small Molecule Recognition

Since these proteins can assemble into pentameric coiled-coils with a hydrophobic pore capable of recognizing guest molecules, we assesses their ability to bind curcumin (CCM).[16] His_6-C demonstrates a fluorescence signal of 78.9 ±16 RFU in the presence of CCM, indicative of binding (**Figure 4**, Supporting Information Table S2). In the presence of Zn(II), the fluorescence signal for His_6-C doubles with an intensity of 166.9 ±9 RFU, suggesting enhanced binding (Figure 4, Supporting Information Table S2). By contrast, a two-fold reduction in fluorescence is observed in the presence of Ni(II) (Figure 4, Supporting Information Table S2). His_6-T40A exhibits better binding to CCM, presumably due to the enhanced helical structure and stability relative to His_6-C with a fluorescence intensity of 101 ± 6.6 RFU (Figure 4, Supporting Information Table S2).[16] While the level of fluorescence is slightly enhanced in the presence of Zn(II), there is a five-fold loss in fluorescence in the presence of Ni(II). The abilities of His_6-C and His_6-T40A to recognize CCM appear to be linked to the structure. Since Zn(II) is able to confer helical conformation in the proteins, binding is observed, however Ni(II) disrupts the helix, leading to a loss in CCM binding. His_6-L44A, by itself, is unable to bind to CCM and no characteristic fluorescence is observed. Surprisingly, in the presence of Zn(II), His_6-L44A exhibits binding to CCM, as demonstrated by a fluorescence signal of 60 ± 7.5 RFU, affirming the formation of α-helical conformation from CD (Figure 4, Supporting Information Table S2). Essentially, His_6-L44A in the presence of Zn(II) is able to exhibit nearly identical binding to His_6-C, indicating that Zn(II) can not only trigger α-helical conformation from random coil structure but also enable the pentameric assembly to facilitate binding to CCM. Minimal binding is observed in the presence of Ni(II), confirming that the Ni(II) does not stabilize the helical structure and rather induces aggregation.

3. Conclusions

Our studies demonstrate that the differential binding of divalent metals to coiled-coils bearing an N-terminal hexahistidine tag can influence overall structure, small molecule binding, and recognition as well as supramolecular assembly into fibers. While Zn(II) significantly improves helical structure and stability as observed in other peptide systems, Ni(II) disrupts helical integrity.[12,14] This translates into enhanced fiber formation in the presence of Zn(II) for coiled-coils with greater than 50% helical content and mesoscale aggregation in the presence of

Table 2. Summary of ATR-FTIR data.

Protein	No Metal [cm^{-1}]		Zn (II) [cm^{-1}]		Ni (II) [cm^{-1}]	
	PB	D_2O	PB	D_2O	PB	D_2O
His_6-C	1653	1653	1653	1653/48	1653	1653/47
His_6-T40A	1653	1653	1653	1653/48	1653	1653/47
His_6-L44A	1653	1652/47	1653	1653/48	1653	1653/47

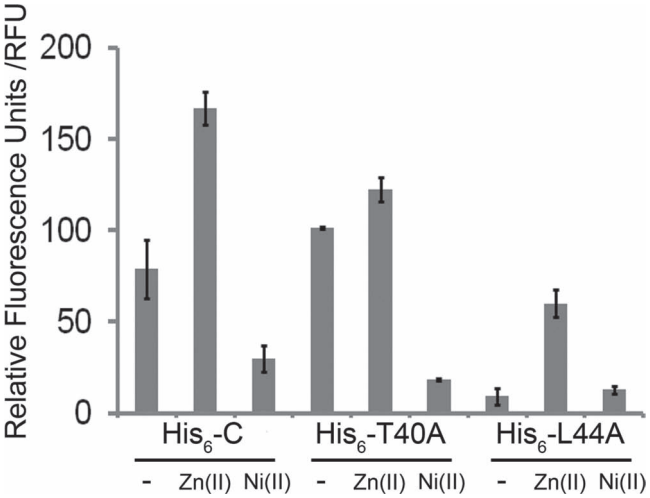

Figure 4. Curcumin fluorescence of His_6-C, His_6-T40A, and His_6-L44A in the absence and presence Zn(II) and Ni(II) metals.

Ni(II). The effect of the metals on the conformation is further confirmed by the investigation of binding to CCM. In the presence of Zn(II), CCM recognition is maintained as it stabilizes the α-helical conformation for His_6-C and His_6-T40A, while in the presence of Ni(II), the helix is destabilized leading to loss in binding. Remarkably, Zn(II) is able to trigger binding to CCM of His_6-L44A from no detectable binding through the induction of helical conformation. This system provides a unique advantage as the precise position of His residues within the hydrophobic core of the helical polypeptide is not needed, leaving the room for metal recognition and small molecule binding. At least for the coiled-coils, an N-terminal hexahistidine tag appears to have a very large influence on protein secondary structure and stability while interacting with divalent metals. Contrastingly, a naturally occurring zinc finger motif possesses a four residue metal coordination site arising from core peptide backbone and influencing its structure and function.[25] Our work provides insight onto further design of protein-based fiber assemblies in addition to the control over folding and release of small molecule by external trigger. Hence, these assemblies can be further exploited as robust platforms for triggered small molecule release and metal-based nanostructures.

4. Experimental Section

Materials: Sodium phosphate (monobasic and dibasic), nickel chloride, zinc chloride, trizma base, and nickel-nitrilotriacetic acid resins were purchased from Sigma-Aldrich. Ampicillin, isopropyl-β-D-thiogalactopyranoside (IPTG), tryptone, urea, and sodium chloride were obtained from Fisher Scientific. Yeast extract, methanol, and CCM were from Acros and the MicroBCA kit was obtained from Pierce. EDTA was purchased from VWR. Deuterium oxide was purchased from MP Biomedicals. Factor Xa cleavage capture kit was obtained from EMD chemicals.

Expression and Purification: The His_6-C gene in pQE9 vector (gift from Kechun Zhang) was used to generate the His_6-T40A and His_6-L44A by site-directed mutagenesis as described previously.[16] His_6-C^{Xa} was generated by amplifying the pQE9/His_6-C gene with the following primers: 5′-GCATGGGATCCATCGAAGGTCGCGCGCCGCAGATGCTGCGT-3′ and 5′-GCATGAAGCTTTGAGGTGTTTTTCAGGAAGG-3′. The amplified gene was cloned at the BamHI and HindIII site of the pQE9 vector. The His_6-T40A^{Xa} and His_6-L44A^{Xa} constructs were obtained by site-directed mutagenesis of the pQE9/His_6-C^{Xa} as previously described.[16] These gene constructs were expressed in XL-1 blue cells. The cultures were grown in 1 L Luria Bertani (LB) medium with ampicillin (1 mM) at 37 °C and 250 rpm. At an optical density of 1.0 at 600 nm, IPTG (1 mM) was added and incubated for 3 h at 37 °C and 250 rpm. Purification under denaturing conditions was carried out using urea (8 M), sodium phosphate monobasic (0.1 M), and trizma base (10 mM) buffer (pH 8.0). The soluble crude lysate was bound to Ni-NTA beads and allowed to equilibrate for 3 h at 4 °C. The proteins were eluted using buffers of decreasing pH's of 5.47, 5.12, and 4.44. Pure fractions were refolded by dialysis in phosphate buffered saline (100 mM PBS, pH 8.0). Factor Xa protease cleavage reaction was performed on purified His_6-C^{Xa}, His_6-T40A^{Xa} and His_6-L44A^{Xa} proteins to produce C^{Xa}, T40A^{Xa} and L44A^{Xa} as specified in the manufacturer's manual. MicroBCA kit was used to estimate protein concentration with bovine serum albumin (BSA) as a standard.

Metal Binding: Divalent metals (Zn(II) and Ni(II)) were added so that the final concentration of the protein and the metals were 10 μM (100 mM PBS) and 100 μM (dH_2O) respectively. Proteins were incubated with appropriate metals overnight at 4 °C to facilitate binding. To sequester the metal, a final concentration of EDTA (1 mM) was used.[12]

Circular Dichroism (CD) Spectroscopy: Wavelength scans were measured from 200–250 nm and temperature scans were monitored with respect to 222 nm over a temperature range of 5 to 85 °C using Jasco J-815 CD spectrometer.[16] Conversion of raw ellipticity (Θ) values to mean molar residue ellipticity (Θ_{MRE}) was calculated as $\Theta_{MRE} = \Theta/(10cpl)$, where c denotes the protein concentration in molar, p denotes the path length in cm, and l denotes the length of protein.[26]

The% helicity of the protein was measured as $f = 100((\Theta)_{222}/(\Theta_{max})_{222})$, where $(\Theta_{max})_{222} = -40\,000(1 - (2.5/n))$, and n = total length of the peptide chain.[27]

The fraction folded of the protein was determined as $F = (\Theta_A - \Theta_U)/(\Theta_N - \Theta_U)$, where Θ_A is the observed MRE value. The Θ_U and Θ_N are the MRE values at the unfolded and folded states respectively.[28] The T_m was estimated by taking the first derivative of the denaturation curve.[29] All CD measurements were performed at 10 μM protein concentration in PBS (100 mM PBS, pH 8.0) in duplicate.

Isothermal Titration Calorimetry (ITC): The metal to protein binding stoichiometry was determined by performing isothermal titration calorimetry using a Microcal VP-ITC instrument. Either Zn (II) (500 μM in 10 mM phosphate buffer, pH 8.0) or Ni (II) (200 μM in 10 mM phosphate buffer, pH 8.0) was titrated into the protein solution (10 μM in 10 mM phosphate buffer, pH 8.0). A series of 10 μL injections containing the metal solution was delivered to the protein solution at 25 °C with constant stirring at 307 rpm. Heat of dilution due to metal injected into the buffer was subtracted as background and the data was fit to one-binding-site model using Origin-7 software.[12] The data represent the average of two separate trials.

Transmission Electron Microscopy (TEM): A Phillips CM-100 transmission electron microscope was used to view the supramolecular protein structure. Approximately 2 μL of protein (10 μM in 10 mM PB, pH 8.0) was added on copper grids and blotted out using filter paper. The sample was negatively stained by adding 3 μL of 1% uranyl acetate, blotted using filter paper, and dried at room temperature.[1] ImageJ software was used to measure the dimensions of the fibers and particles.

Small Angle X-Ray Scattering (SAXS): The SAXS experiments were performed at the National Synchrotron Light Source facility at Brookhaven National Lab, using the undulator-based X9 end station. An X-ray wavelength of 0.0856 nm was selected. Data was recorded on charge-coupled device (CCD) area detectors using a 20 s exposure time and integrated in software into 1D line profiles. The measurement was done by adding lyophilized protein sample (0.4 mg) to a capillary tube of 1 mm diameter (from Charles Supper) and data were background

corrected using an empty capillary. Curve fitting to the cylindrical form factor (diameter = 20 Å; length = 400 Å) was done using the NIST Center for Neutron Research analysis software.[19,20,30]

Attenuated Total Reflectance Fourier Transform Infrared Spectroscopy (ATR-FTIR): FTIR experiments were performed using Perkin Elmer System 2000 FT-IR with DuraSamplIR II^T diamond ATR accessory. 20 μL of peptide solution (2 mg mL^{-1} in 10 mM PB, pH 8.0) were added on the diamond ATR surface and dried under nitrogen until a thin layer was formed. The spectrum (128 scans) was measured at room temperature over a range of 4000–400 cm^{-1} with 0.5 cm^{-1} resolution. In the case of deuterium exchange (D_2O) experiments, the lyophilized protein (in the absence and presence of metals) was suspended in D_2O and the spectrum was recorded immediately. Fourier self-deconvolution was performed using a Lorentzian line shape function of gamma = 1. Baseline correction of the amide I region between 1700–1600 cm^{-1} was done using PeakFit software. Assigning the peaks to the baseline corrected spectra was performed by curve fitting to a Gaussian constrained area profile using the PeakFit software.[31] All readings represent the average of two trials.

Fluorescence: CCM fluorescence measurements were carried out using 10 μM of protein (10 mM PB, pH 8.0) in the absence and presence of 100 μM of metals (Zn (II) and Ni (II)) at room temperature. Approximately CCM (50 μM) in 10 mM PB (pH 8.0) and methanol (0.5%) was added to the protein in the absence and presence of metals and incubated for 2 h at room temperature. Fluorescence was measured using SpectraMax Plus M2 instrument. The wavelength was excited at 420 nm and emission wavelength was measured over a range of 450–600 nm.[16] The buffer in the absence and presence of metals upon binding to CCM did not produce any fluorescence. All proteins exhibited a maximum emission peak around 500 nm.

Supporting Information

Supporting Information is available from the Wiley Online Library or from the author.

Acknowledgements

The authors thank Ronald McLurkin, Chin Lin, Jorge Morales, Kevin Yager, Eric Roth, David Kaplan, and Xiao Hu for technical assistance and critical insight into the experiments and manuscript. This work was supported by the AFOSR (FA-9550-07-1-0060 and FA-9550-08-1-0266), ARO (W911NF-11-1-0449), and in part by the NSF MRSEC Program under Award Number DMR-0820341. Small angle X-ray scattering experiments performed at the National Synchrotron Light Source, Center for Functional Nanomaterials, Brookhaven National Laboratory, were supported by the U.S. Department of Energy, Office of Basic Energy Sciences, under Contract No. DE-AC02-98CH10886. Electron microscopic analysis of this work was supported by the U.S. Department of Energy, Office of Basic Energy Sciences, Division of Materials Sciences and Engineering under Award No. DE-FG-02-01ER45935.

Received: July 15, 2011
Revised: January 1, 2012
Published online: February 20, 2012

[1] M. J. Pandya, G. M. Spooner, M. Sunde, J. R. Thorpe, A. Rodger, D. N. Woolfson, *Biochemistry* **2000**, *39*, 8728.
[2] D. N. Woolfson, M. G. Ryadnov, *Curr. Opin. Chem. Biol.* **2006**, *10*, 559.
[3] M. T. Klem, M. Young, T. Douglas, *J. Mater. Chem.* **2008**, *18*, 3821.
[4] Y. S. Nam, T. Shin, H. Park, A. P. Magyar, K. Choi, G. Fantner, K. A. Nelson, A. M. Belcher, *J. Am. Chem. Soc.* **2010**, *132*, 1462.
[5] J. M. Slocik, F. Tam, N. J. Halas, R. R. Naik, *Nano Lett.* **2007**, *7*, 1054.
[6] A. S. Blum, C. M. Soto, K. E. Sapsford, C. D. Wilson, M. H. Moore, B. R. Ratna, *Biosens. Bioelectron.* **2011**, *26*, 2852.
[7] K. Pagel, S. C. Wagner, K. Samedov, H. von Berlepsch, C. Böttcher, B. Koksch, *J. Am. Chem. Soc.* **2006**, *128*, 2196.
[8] R. A. Kammerer, D. Kostrewa, J. Zurdo, A. Detken, C. García-Echeverría, J. D. Green, S. A. Müller, B. H. Meier, F. K. Winkler, C. M. Dobson, M. O. Steinmetz, *Proc. Natl. Acad. Sci. USA* **2004**, *101*, 4435.
[9] B. C. Kovaric, B. Kokona, A. D. Schwab, M. A. Twomey, J. C. de Paula, R. Fairman, *J. Am. Chem. Soc.* **2006**, *128*, 4166.
[10] S. N. Dublin, V. P. Conticello, *J. Am. Chem. Soc.* **2007**, *130*, 49.
[11] S. K. Gunasekar, J. S. Haghpanah, J. K. Montclare, *Polym. Adv. Technol.* **2008**, *19*, 454.
[12] E. Cerasoli, B. K. Sharpe, D. N. Woolfson, *J. Am. Chem. Soc.* **2005**, *127*, 15008.
[13] A. S. Ulrich, M. Otter, C. G. Glabe, D. Hoekstra, *J. Biol. Chem.* **1998**, *273*, 16748.
[14] T. Kiyokawa, K. Kanaori, K. Tajima, M. Koike, T. Mizuno, J. I. Oku, T. Tanaka, *J. Pept. Res.* **2004**, *63*, 347.
[15] R. S. Signarvic, W. F. DeGrado, *J. Am. Chem. Soc.* **2009**, *131*, 3377.
[16] S. K. Gunasekar, M. Asnani, C. Limbad, J. S. Haghpanah, W. Hom, H. Barra, S. Nanda, M. Lu, J. K. Montclare, *Biochemistry* **2009**, *48*, 8559.
[17] M. M. Long, D. W. Urry, W. Stoeckenius, *Biochem. Biophys. Res. Commun.* **1977**, *75*, 725.
[18] D. W. H. Frost, C. M. Yip, A. Chakrabartty, *Pept. Sci.* **2005**, *80*, 26.
[19] A. Guinier, G. Fournet, *Small-Angle Scattering of X-rays*, John Wiley & Sons, New York **1955**.
[20] S. Kline, *J. Appl. Crystallogr.* **2006**, *39*, 895.
[21] J. T. Pelton, L. R. McLean, *Anal. Biochem.* **2000**, *277*, 167.
[22] X. Chen, D. P. Knight, Z. Shao, F. Vollrath, *Biochemistry* **2002**, *41*, 14944.
[23] R. Khurana, J. R. Gillespie, A. Talapatra, L. J. Minert, C. Ionescu-Zanetti, I. Millett, A. L. Fink, *Biochemistry* **2001**, *40*, 3525.
[24] M. S. Celej, M. G. D'Andrea, P. T. Campana, G. D. Fidelio, M. L. Bianconi, *Biochem. J.* **2004**, *378*, 1059.
[25] R. Gamsjaeger, C. K. Liew, F. E. Loughlin, M. Crossley, J. P. Mackay, *Trends Biochem. Sci.* **2007**, *32*, 63.
[26] D. L. Lee, C. T. Mant, R. S. Hodges, *J. Biol. Chem.* **2003**, *278*, 22918.
[27] B. Forood, E. J. Feliciano, K. P. Nambiar, *Proc. Natl. Acad. Sci. USA* **1993**, *90*, 838.
[28] S. L. Flaugh, I. A. Mills, J. King, *J. Biol. Chem.* **2006**, *281*, 30782.
[29] N. J. Greenfield, *Nat. Protoc.* **2007**, *1*, 2527
[30] A. Altunbas, N. Sharma, M. S. Lamm, C. Yan, R. P. Nagarkar, J. P. Schneider, D. J. Pochan, *ACS Nano* **2009**, *4*, 181.
[31] X. Hu, D. Kaplan, P. Cebe, *Macromolecules* **2006**, *39*, 6161.